Engineering Journal issn: 0125-8281

Article

Performance Improvement for Germanium-Based Near-Field Thermophotovoltaic Converter

Natkamon Pongtemsuk[1,a], Roytor Charoensin-O-Larn[1,b], and Naphatsorn Vongsoasup[1,2,c,*]

1 Department of Mechanical Engineering, Faculty of Engineering, Chulalongkorn University, Thailand
2 Micro/Nano Electromechanical Integrated Device Research Unit, Faculty of Engineering, Chulalongkorn University, Thailand
E-mail: [a]6570080321@student.chula.ac.th, [b]roytor.c@chula.ac.th,
[c,*]naphatsorn.v@chula.ac.th (Corresponding author)

Abstract. Near-field Thermophotovoltaic (NF-TPV) converter utilizes the tunnelling of an evanescent wave to surpass the blackbody limit, enhancing the radiative heat transfer of the TPV converter by several orders of magnitude. One of key challenges for commercial NF-TPV converter is cost reduction. Germanium is known to be a cost-effective material with bandgap energy compatible with a TPV application. In this study, the germanium-based NF-TPV converter is introduced with an addition of air-bridge gap (ABG) at the interface between a TPV cell substrate and a metal back surface reflector (BSR) as a strategy to improve sub-bandgap photon utilization. Effects of air-bridge gap and germanium substrate thickness on radiative heat fluxes and converter performance are investigated. At the radiator temperature of 1400 K and the optimum air-bridge gap thickness of 1300 nm, system efficiency of NF-TPV converter increases from 17.16% to 24.98% for a 175 μm thick TPV cell, and from 16.73% to 31.39% for a 40 μm thick TPV cell under moderate surface passivation. In addition, the converter's performance under varying radiator temperature is analysed. This study demonstrates the potential of the air-bridge gap to optimize NF-TPV converter performance.

Keywords: Near-field effect, germanium thermophotovoltaic converter, system efficiency, air-bridge gap, back surface reflector.

ENGINEERING JOURNAL Volume 29 Issue 4
Received 30 December 2024
Accepted 18 April 2025
Published 30 April 2025
Online at https://engj.org/
DOI:10.4186/ej.2025.29.4.85

DOI:10.4186/ej.2025.29.4.85

1. Introduction

Thermophotovoltaic (TPV) converter generates electricity from the heat in the form of thermal radiation through the generation of electron-hole pairs (EHPs), replacing the solar irradiance in conventional solar cells with a high temperature radiator as a thermal radiation source. The radiator extracts heat from thermal sources and transfers it to the TPV cell in the form of thermal radiation across the vacuum space. Various thermal sources can be used to heat the radiator to high temperature such as pumped molten silicon in pipes used in the thermal energy storage application [1], steel industry waste heat recovery [2], and concentrated light used in the solar thermophotovoltaic application [3], etc. Together with the increasing demand for renewable energy [1], flexibility in thermal sources of the TPV converter attracts many researchers to focus on understanding the theory of TPV converter and conducting a proof-of-concept studies for various design of system with the TPV converter as an energy conversion device, aiming to improve the TPV converter performance. Conventionally, the TPV converter operates in far-field regime which has a propagating wave as a dominant mechanism of radiative transfer. Therefore, the power output of the TPV converter is limited by the Planck distribution. It is known that the phenomenon called tunnelling of evanescent waves occurs between closely spaced bodies, with the separation distance in the order of the thermal radiation wavelength calculated from Wien's displacement law. This phenomenon could enhance the radiative exchange between bodies to orders of magnitude beyond the Planck's blackbody limit [4-6]. Therefore, this near-field effect could be incorporated to increase the power output of the TPV converter. A near-field thermophotovoltaic (NF-TPV) converter is a TPV converter coupled with the near-field effect to enhance its performance. The NF-TPV converter has been developed both theoretically and experimentally for over a decade. Recently, a convincing experimental study using an InGaAs-based TPV cell reported 5000 W/m^2 power output with 6.8% efficiency [7].

One of the most important aspects of TPV converter research is cost reduction. Most reported high performance TPV converters use III-V materials as a cell substrate. Compared to the III-V materials, Germanium is more abundant and cheaper with a comparable bandgap energy of 0.661 eV which is compatible with a temperature range of TPV application [8]. Typically, Germanium PV cell is used in a multijunction structure such as the PV cell used in a space application. There are continuous efforts to use a Germanium-based cell in the TPV converter [8-11]. In the early 2000s, Nagashima et al. [9] conducted a study of a back contact type Germanium-based TPV converter. The highest theoretical efficiency of 25% was reported. Fernandez et al. [10] applied a passivation layer of a-Si/SiO_2 to Ge-based TPV cell back side designs to improve surface passivation quality and substrate characteristics leading to 16.5% efficiency. In a recent study, Martin et al [11] proposed a fabrication method for several characterizations of Ge-based TPV converter, achieving an efficiency of 23.2%. The strategies for further improvement of the TPV converter performance were also reported in their work showing the potential of the Ge-based converters. Consequently, the understanding of the radiative heat transfer characteristics of the Ge-based NF-TPV converter and the evaluation of its performance would be a crucial step to commercialize the TPV converter.

For a TPV cell, the radiative flux absorbed in the sub-bandgap frequency range does not generate electron-hole pairs. These sub-bandgap photons result in a parasitic heat absorption which is a burden to the thermal management system leading to lowered converter efficiency. In the doped semiconductor with relatively large thickness such as Ge, the semiconductor exhibits high sub-bandgap absorption due to free-carrier in the infrared region. Tunnelling of evanescent waves greatly enhance this loss. Therefore, the mitigation of this loss should be considered for the Ge-based NF-TPV converter. Typically, a back surface reflector (BSR) is used to deal with this loss by reflecting the unabsorbed sub-bandgap photon back to reheat the radiator. However, various spectral control methods could be employed to further enhance sub-bandgap photon utilization. Inoue et al. [12] demonstrated the scheme of Si intermediate layer to be placed between a radiator and an InGaAs TPV cell to suppress absorption of the surface phonon polariton (SPhP) in the sub-bandgap region. This phenomenon is caused by the evanescent waves coupling with the lattice vibration resonance frequencies of polar materials such as III-V materials. Placing the non-polar material (i.e. intrinsic Si) which does not support the SPhP in the sub-bandgap region helps mitigating this loss. Their scheme achieved a theoretical power density of higher than 5x104 W/m^2. Fan et al. [13] proposed an insertion of an air-bridge gap (ABG) between the semiconductor substrate layer of the thin-film InGaAs TPV cell and the back surface reflector (BSR). This modification can increase the sub-bandgap reflection up to 98.5% resulting in an 8% increase in system efficiency compared to the configuration with only the back surface reflector. Similarly, Arulanandam et al. [14] implemented a patterned dielectric back contact (PDBC) structure using SU-8 as dielectric and Au point contact. The structure achieved 96.5% sub-bandgap reflectivity showing 1% improvement compared to the Au only back contact.

In this study, with the aim to design the Ge-based NF-TPV converter, we investigate the performance characteristics of NF-TPV converter. The reported parameters include radiative heat fluxes and performance matrices including J-V characteristics, power output density, and system efficiency. An air-bridge gap (ABG) is chosen as the strategy to improve the sub-bandgap photon utilization. In addition, the effects of the air-bridge gap and the thickness of Ge substrate on the radiative heat transfer and the TPV converter performance are clarified.

2. Methods

The performance analysis is carried out through two models. First, the radiative heat transfer behaviour within the converter, including the incident and absorbed radiative heat flux, is determined. Then, the photocurrent density is calculated by the performance evaluation model while considering the recombination mechanism. Finally, using the radiative heat flux and the photocurrent density, the converter's power output density and the system efficiency are determined.

2.1. Radiative Heat Flux Model

The NF-TPV converter illustrated in Fig. 1 consists of the radiator layer, vacuum space, and TPV cell and is considered as 1-D multilayer planar geometry in the radiative heat transfer calculation. The absorbed radiative heat flux by the layer i from the thermal source layer j, denoted as Q_{ij} is determined by the difference between the Poynting flux evaluated at Z_i and Z_{i-1}. Using the fluctuational electrodynamics formalism [15], Q_{ij} is expressed as follows:

$$Q_{ij} = \int_0^\infty \left[\Theta(\omega, T_j, \mu_j) - \Theta(\omega, T_i, \mu_i)\right]\phi_{ij}(\omega)d\omega \quad (1)$$

$$\Theta(\omega, T, \mu) = \begin{cases} \dfrac{\hbar\omega}{\exp\left(\dfrac{\hbar\omega - \mu}{k_b T}\right) - 1}; \omega \geq \omega_g \\ \dfrac{\hbar\omega}{\exp\left(\dfrac{\hbar\omega}{k_b T}\right) - 1}; \omega < \omega_g \end{cases} \quad (2)$$

$\phi_{ij}(\omega)$ represents the portion of the absorbed energy flux in the layer i radiated from the thermal source j. It can be determined through the difference between the transmission factor [16], evaluated at top (Z_{i-1}) and bottom (Z_i) interfaces of the layer i. The open-source software based on the Rigorous Coupled-Wave Analysis (RCWA) with the scattering matrix framework and fluctuation electrodynamics [16] is used to calculate these transmission factors. The mean energy of a Planck oscillator corresponding to the angular frequency ω and the temperature T, modified to include the chemical potential μ, is denoted as $\Theta(\omega, T, \mu)$. The chemical potential is considered as the multiplication of the elementary charge q and the bias voltage V. The expression for the $\Theta(\omega, T, \mu)$ is as shown in Eq. (2). Notably, the chemical potential is included only when the angular frequency is greater than or equal to the bandgap frequency ω_g of the substrate layer. This way, the effect of the external luminescent of the semiconductor substrate can be included in the model. $\hbar$ is the reduced Planck constant and k_b is the Boltzmann constant.

2.2. Performance Evaluation Model

From the radiative heat flux model explained above, we can calculate both the above-bandgap absorbed radiative heat flux and the external luminescence of the Ge substrate layer. The former represents the fraction of energy contributing to the generation of electron-hole pairs (EHPs), which is used to calculate the photogeneration rate G_a. The internal quantum efficiency (IQE) is assumed to be 100% meaning that every above-bandgap absorbed photon contributes to EHPs generation. The latter is used to calculate the radiative recombination rates G_e, or the re-emitted photons from the Ge substrate layer. Losses caused by the non-radiative recombination mechanisms are accounted for in R(V). Finally, the photocurrent density J(V) can be expressed as [17]:

$$J(V) = q\{G_a - G_e(V) - R(V)\} \quad (3)$$

$$G_a = \frac{1}{\hbar\omega}\int_{\omega_g}^{\infty} \Theta(\omega, T_0, 0)\phi_{20}(\omega)d\omega \quad (4)$$

$$G_e = \int_{\omega_g}^{\infty} \Theta(\omega, T_2, \mu_2)\phi_{02}(\omega)d\omega \quad (5)$$

It is noted that radiative recombination rate depends on the bias voltage V, as the chemical potential $\mu_2 = qV$, as described above. The term $q\{G_a - G_e(V)\}$ is a photocurrent generation rate which represents a photocurrent density without a consideration for non-radiative recombination losses. R(V) accounts for the bulk recombination mechanism, consisting of Auger (R_{auger}) and Shockley-Read-Hall (R_{SRH}) recombination rates, and the surface recombination rate (R_{surf}) as described in Eq. (6)-(9).

$$R(V) = R_{auger}(V) + R_{SRH}(V) + R_{surf}(V) \quad (6)$$

$$R_{auger}(V) = \sum_j^{n,p}\left(C_n n + C_p p\right)(np - n_i^2)t_j \quad (7)$$

$$R_{SRH}(V) = \sum_j^{n,p}\frac{(np - n_i^2)}{(n + n_{t,b})\tau_p + \left(p + p_{t,b}\right)\tau_n}t_j \quad (8)$$

$$R_{surf}(V) = \sum_j^{n,p}\frac{(np - n_i^2)}{(n + n_{t,s})S_{p,j} + \left(p + p_{t,s}\right)/S_{n,j}} \quad (9)$$

Each recombination rate is summed over n- and p-region of the Ge substrate layer. To calculate the recombination rates in Eq. *(7)-(9)*, recombination parameters of the Ge are needed including Auger coefficients for electrons C_n and holes C_p, bulk lifetimes for electrons τ_n and holes τ_p, and surface recombination velocities at region j for electrons $S_{n,j}$ and holes $S_{p,j}$. The

DOI:10.4186/ej.2025.29.4.85

bulk trap concentrations for electrons $n_{t,b}$ and holes $p_{t,b}$ and the surface trap concentrations for electrons $n_{t,s}$ and holes $p_{t,s}$ are considered to be the same as intrinsic carrier concentrations n_i [17]. These parameters are obtained from [18]. The thickness of each region of the substrate layer of the TPV cell t_j is only considered for the bulk recombination rates. These non-radiative recombination rates are the function of V by the relation written in Eq. (10), which can be used to calculate the value of concentrations of electrons n and holes p.

$$pn=p_0 n_0 \exp\left(\frac{qV}{k_b T_2}\right) \quad (10)$$

where n_0 and p_0 represent the equilibrium concentrations of electrons and holes., respectively Surface recombination velocity for both n- and p- region are selected to be 1000 cm/s [19]. The power output density is obtained by multiplying the photocurrent density by the bias voltage. The system efficiency *(*S.E.*)* is defined as:

$$\text{S.E.} = \frac{J(V)\times V}{Q_{inc}} \quad (11)$$

where Q_{inc} represents the total radiative heat flux incident on the TPV cell including Ge substrate, air-bridge gap and back surface reflector layers.

3. Results and Discussions

Figure 1 illustrates the NF-TPV converter considered in this study. A bulk tungsten (W) radiator with a constant temperature of 1400 K is used as a thermal radiation source. A TPV cell consists of a p-type Germanium (Ge) cell substrate at 300 K with 2×10^{15}cm^{-3} acceptor concentration. Two substrate thicknesses are considered. A "thick cell" refers to a typical thickness of commercial Ge wafer with t_{cell} = 175 µm. A "thin cell" refers to a high-performance Ge-based cell with t_{cell} = 40 µm [19]. An n-type Germanium layer is not included in both the radiative heat flux model and the performance evaluation model since the typical thickness of a few hundred nanometres is negligible compared to the p-type region. The radiator and the TPV cell are separated by a distance d = 100 nm. Optical properties for W are obtained from [20].

Optical properties of Ge in the above-bandgap region are obtained from [21] while the free-carrier absorption mechanism affected by the acceptor concentrations are obtained based on [22]. Two TPV cell configurations are analysed. The first configuration is the TPV cell with only the back surface reflector (BSR). The BSR is made from aluminium (Al) with a thickness of 1 µm. Optical properties of the BSR are obtained from [23]. The second configuration consists of the TPV cell with both the air-bridge gap (ABG) and the BSR. The thickness of the ABG (t_{abg}) is varied.

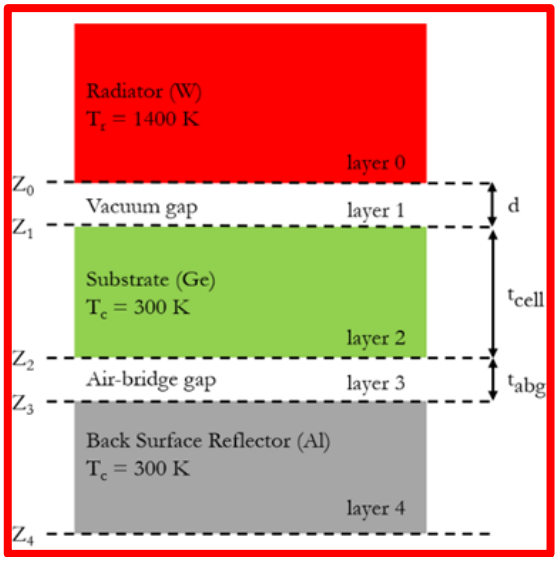

Fig. 1. A schematic diagram of near-field thermophotovoltaic (NF-TPV) converter.

3.1. Effects of Air-Bridge gap on Radiative Heat Fluxes in NF-TPV Converter

Figure 2 illustrates the spectral radiative heat fluxes within the converter, including the incident radiative heat flux on the TPV cell from the radiator (q_{inc}), the absorbed radiative heat flux in the Ge substrate (q_{cell}), and the absorbed radiative heat flux in the Al BSR (q_{bsr}). The incident radiative heat flux is absorbed by either the Ge substrate or the Al BSR, as these are the only absorbing layers in the TPV cell. Therefore, the sum between absorbed flux in these two layers is equal to the incident flux ($q_{inc} = q_{cell} + q_{bsr}$). For the configuration of the 175 µm cell with only the BSR, the sub-bandgap incident radiative heat flux is comparable to that of the above-bandgap region. The free-carrier absorption mechanism of the Ge substrate causes a portion of this sub-bandgap flux to be accumulated in this layer while the majority is absorbed in the Al BSR. These absorbed sub-bandgap radiative heat fluxes do not contribute to the electricity generation but result in the parasitic heat absorption. Conversely, Ge substrate absorbs most of the radiative heat flux in the above-bandgap region, except for small portion near the bandgap frequency. The relatively large amount of sub-bandgap heat absorption exhibits the potential for the sub-bandgap photon utilization. Subsequently, when the air-bridge gap is inserted in the NF-TPV converter, a significant change in radiative heat flux characteristics is observed as shown in Fig. 2 (a)-(c). In the above-bandgap region, as the air-bridge gap thickness (t_{abg}) increases, the slight increases in both incident and absorbed radiative heat fluxes are observed near the bandgap frequency of $1.004\text{x}10^{15}$ rad/s (i.e. 0.661 eV). These increases are likely due to weak absorption near the bandgap frequency of the Ge substrate which is an indirect bandgap semiconductor. As the frequency approaches $1.2\text{x}10^{15}$ rad/s, both fluxes are seen to be unaffected by the air-bridge gap. In the sub-bandgap region, a noticeable reduction in the incident radiative heat

flux is observed as the t_{abg} increases as shown in Fig. 2(a). This reduction is due to improved reflectivity of the NF-TPV converter specifically the high reflectivity at the interface between the Ge substrate and the air-bridge gap. Nevertheless, these reflected sub-bandgap photons are partly reabsorbed in the Ge substrate as increased absorption in this layer is observed in Fig. 2(b). The absorbed radiative heat flux in the BSR is greatly reduced when the t_{abg} is 500 nm. As shown in Fig. 2(c), it is almost zero as the t_{abg} reaches 1300 nm. To quantify improvement of the reflectivity, the reflectivity of the converter is calculated using Rigorous Coupled-Wave Analysis (RCWA) [24]. As shown in Fig. 3(a), the reflectivity of the TPV cell with the air-bridge gap of 1300 nm is increased by approximately 3.5% compared to the converter with only the BSR across the whole sub-bandgap region. It is noted that the above-bandgap reflectivity is unaffected by the air-bridge gap addition. The radiative heat fluxes when the Ge substrate thickness is reduced to 40 μm are shown in Fig. 2(d)-(f). For the configuration of 40 μm cell with only the BSR, the absorbed radiative heat flux in the Ge substrate decreases in both sub- and above-bandgap regions compared to the thick cell caused by the thinner absorbing layer (i.e. Ge substrate layer) as shown in Fig. 2(e). Conversely, the higher absorption in the BSR is observed as shown in Fig. 2(f) since the larger amount of radiative heat flux can reach to the BSR. When the air-bridge gap is inserted, all the radiative heat fluxes exhibit the similar trend with the thick cell. The reflectivity of the thin cell NF-TPV converter is shown in Fig. 3(b). The overall trend is similar to the thick cell. However, the fluctuation is higher due to higher amount of reflected electromagnetic wave as the absorption decreases.

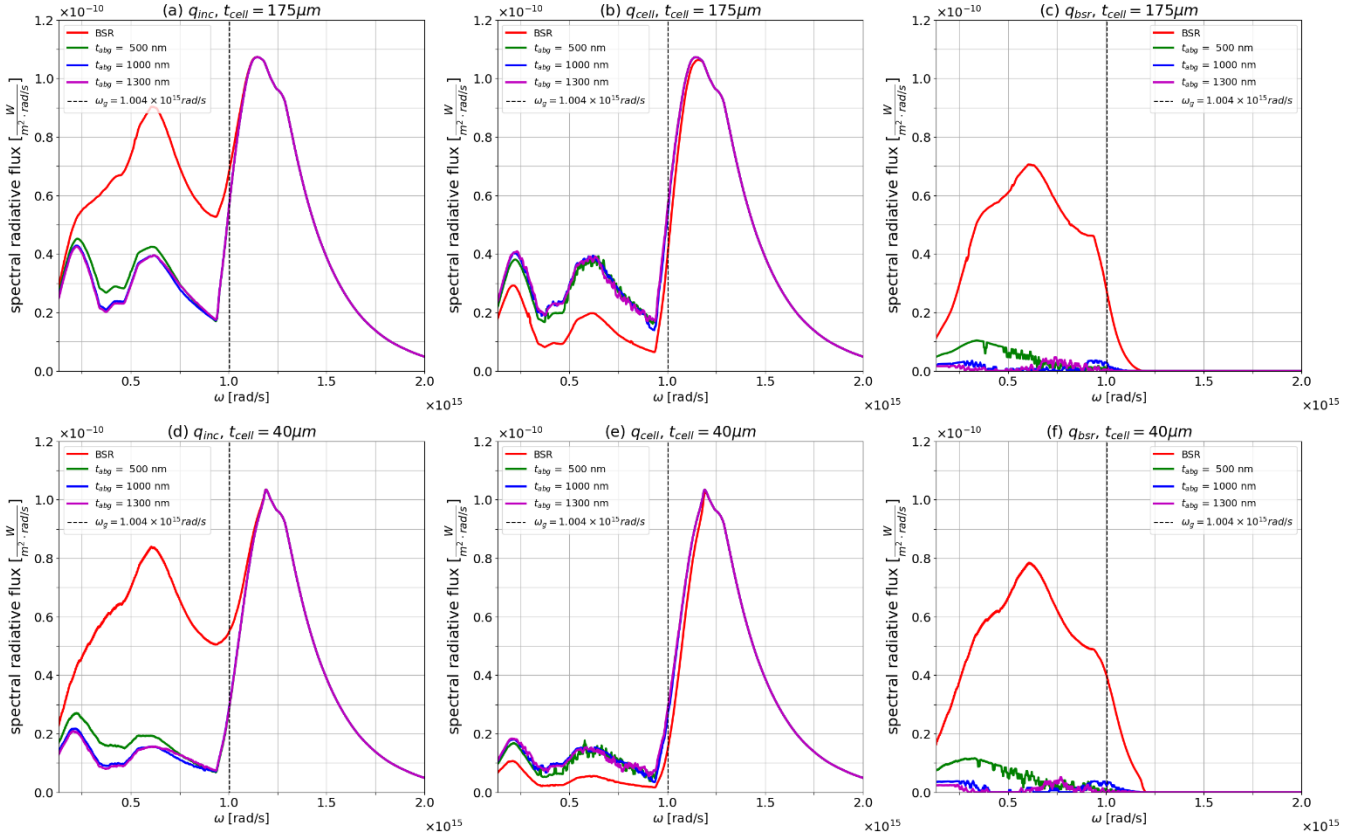

Fig. 2. (a), (d) Spectral incident radiative heat fluxes for 175 μm and 40 μm cells, respectively. (b), (e) Spectral absorbed radiative heat fluxes in the Ge substrate for 175 μm and 40 μm cells, respectively. (c), (f) Spectral absorbed radiative heat fluxes in the BSR for 175 μm and 40 μm cells, respectively.

DOI:10.4186/ej.2025.29.4.85

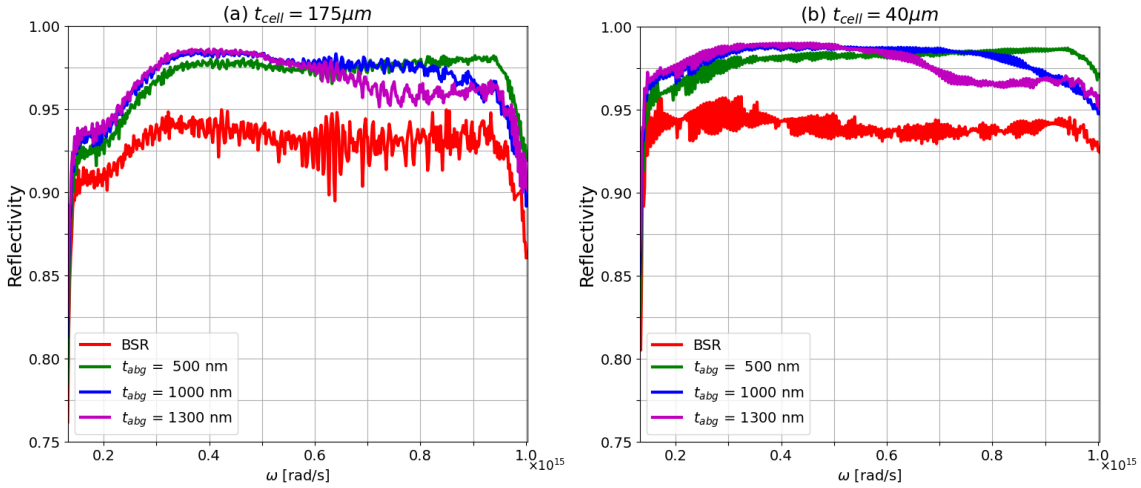

Fig. 3. Sub-bandgap reflectivity of the TPV cell calculated using RCWA.

To optimize the thickness of the air-bridge gap and further investigate the trend of its effects, the total absorbed radiative heat flux in the BSR (Q_{bsr}) is obtained through integrating the spectral radiative heat fluxes shown in Fig. 2(c) and 2(f) over angular frequencies as described in Eq. (12). Alternatively, Q_{bsr} can be calculated through the difference between the total incident radiative heat flux and total absorbed radiative heat flux in the Ge substrate.

$$Q_{bsr} = \int_0^\infty q_{bsr}(\omega)d\omega$$
$$= \int_0^\infty [\Theta(\omega, T_0, 0) - \Theta(\omega, T_4, 0)]\phi_{40}(\omega)d\omega \quad (12)$$

The total absorbed radiative heat fluxes in the BSR with different t_{abg} for thick and thin cells are shown in Fig. 4. The impacts of the air-bridge gap on the radiative heat fluxes of the converter can be observed. For the configuration with only the BSR (t_{abg}= 0), a significant amount of the absorbed radiative heat flux in the BSR indicates high parasitic heat absorption loss. As the air-bridge gap thickness increases, the lower amount of photons reach the BSR. The difference between the 175 µm and the 40 µm cell is due to the different absorbed radiative heat fluxes in the Ge substrate. These changes are saturated approximately at t_{abg}= 1300 nm resulting in about 98% reduction of the heat absorption in the BSR for both 175 µm and 40 µm cells. Further ABG thickness increase does not yield a significant change. Therefore, the optimum t_{abg} is selected as 1300 nm and is referred to as "ABG+BSR" for the remaining of this work.

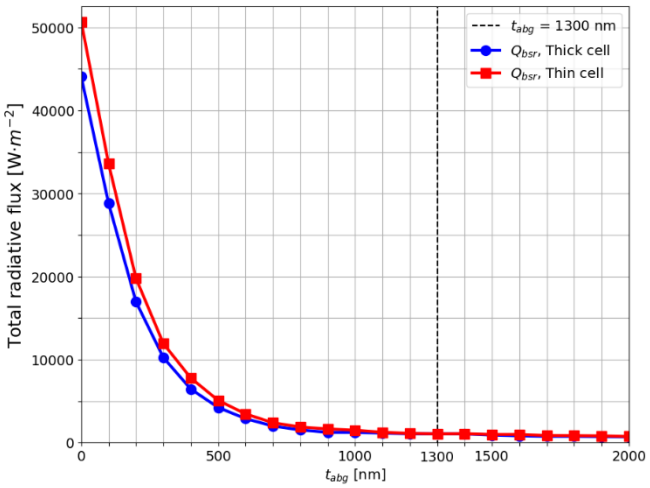

Fig. 4. Total radiative heat fluxes absorbed by the BSR with different t_{abg} for 175 µm and 40 µm cell NF-TPV converters.

3.2. Effects of Air-Bridge Gap on Performance of NF-TPV Converter

Figure 5 illustrates the photocurrent density at different bias voltages, or the J-V characteristics, calculated using Eq. (3). The short-circuit current density (J_{sc}) is obtained by considering the bias voltage of 0 in the Eq. (3). Therefore, this parameter is proportional to the area under the curves in the above-bandgap frequency range of Fig. 2(b) and 2(e). For the 175 µm cell, short-circuit current density of the ABG+BSR configuration is 1.03 times larger than that of the BSR configuration. This is caused by the slightly higher absorbed radiative heat flux near the bandgap frequency of the Ge substrate as previously discussed. This difference persists across the bias voltage range. As the bias voltage increases, the current density decreases, reaching the open-circuit voltage (V_{oc}) at 0.552 V for the ABG+BSR configuration and 0.578 V for the BSR configuration when only the recombination due to the external luminescence of the Ge substrate is considered. When bulk and surface recombination rates are included, the photocurrent

density at non-zero bias voltages drops resulting in open-circuit voltages of 0.396 V for both BSR and ABG+BSR configurations. This indicates significant influence of the bulk and surface recombination as the bias voltage increases.

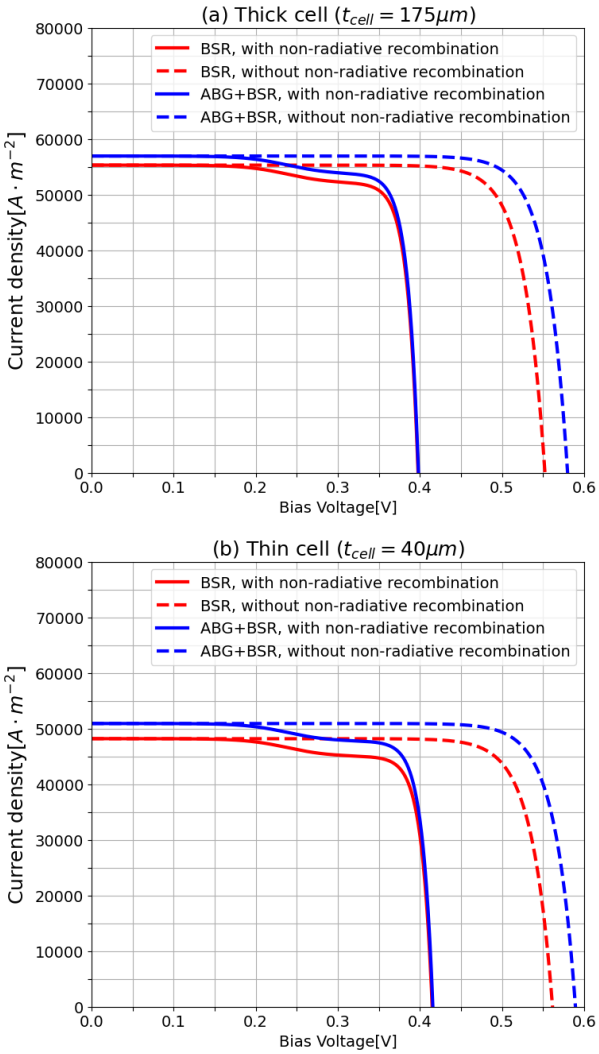

Fig. 5. (a) J-V characteristics of the 175 μm cell converter, (b) J-V characteristics of the 40 μm cell converter, calculated from Eq. (3).

The 40 μm cell exhibits a similar trend to the 175 μm cell. The short-circuit current density is 1.06 times larger when the air-bridge gap is incorporated. The open-circuit voltage, accounting for bulk and surface recombination rates, is 0.414 V, which is larger than that of the 175 μm cell. This is due to the lower bulk recombination rates (R_{auger} and R_{SRH}) which are proportional to the cell thickness as shown in Eq. (7) and Eq. (8). The power output density could be obtained by multiplying the photocurrent density by the bias voltage as shown in Fig. 6. The air-bridge gap slightly improves the power output density for both 175 μm and 40 μm cell converters by increasing the above-bandgap absorbed radiative heat flux in the Ge substrate. Meanwhile, thinner Ge substrate reduce the above-bandgap absorbed radiative heat flux resulting in a slightly lower power output density compared to the thicker cell. However, the thicker substrate results in a shift to the lower maximum power point caused by the higher bulk recombination, as seen by the 0.354 V for 175 μm cell and 0.372 V for 40 μm cell. Maximum power output densities for both configurations are summarized in Table 1. Overall, the power output densities are not significantly affected by the air-bridge gap and the thickness of Ge substrate. However, the significant reduction in the parasitic heat absorption due to lowered sub-bandgap absorbed heat flux in the converter caused by the air-bridge gap is expected to benefit the performance of the converter. The improvement is subsequently quantified by evaluating the parameter that take the effects into account, i.e. the system efficiency as defined in Eq. (11).

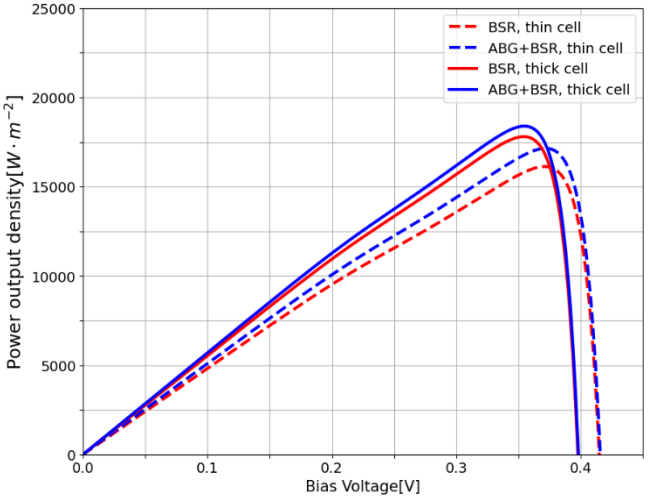

Fig. 6. Power Output Densities of the converter versus the bias voltage for 175 μm and 40 μm cells with and without the air-bridge gap.

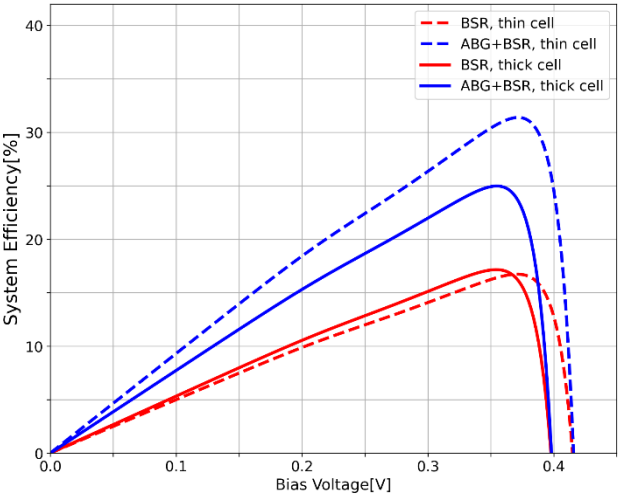

Fig. 7. System efficiencies of the converter versus the bias voltage for 175 μm and 40 μm cells with and without the air-bridge gap.

DOI:10.4186/ej.2025.29.4.85

Table 1. Performance evaluation of NF-TPV converter.

	Incident radiative heat flux, Qinc [W/m²]	Absorbed radiative heat flux, Qcell [W/m²]	Maximum power point bias voltage [V]	Maximum power output density [W/m²]	System efficiency [%]
BSR t_{cell} = 175 μm	103,746	46,615	0.354	17,802	17.16
BSR t_{cell} = 40 μm	96,364	41,543	0.37	16,124	16.73
ABG+BSR t_{cell} = 175 μm	73,614	47,753	0.354	18,389	24.98
ABG+BSR t_{cell} = 40 μm	54,615	43,475	0.372	17,146	31.39

Figure 7 shows system efficiencies of the converter calculated using Eq. (11). For the configuration with only the BSR, the system efficiencies of the 175 μm cell and the 40 μm cell are slightly different due to the comparable incident radiative heat fluxes as shown in Table 1. The maximum system efficiencies are approximately 17% for both 175 μm and 40 μm cells. For the configuration with the air-bridge gap incorporated into the converter; the system efficiencies are significantly improved due to the lowered parasitic heat absorption loss. These improvements result in the maximum system efficiencies of 24.98% for the 175 μm cell and 31.39% for the 40 μm cell. Additionally, the thinning of the Ge substrate is shown to further benefit the converter performance, enhancing the system efficiency by approximately 6.5%.

3.3 Effects of Radiator Temperature on NF-TPV Converter Performance

The system efficiency at different radiator temperatures is illustrated in Fig. 8 to investigate the performance of the converter under varying conditions or different thermal sources. The lower radiator temperature shifts the spectral distribution of the radiative heat transfer towards the longer wavelengths or lower angular frequencies, which is the direction of the Ge sub-bandgap region, leading to the lowered above-bandgap absorbed radiative heat flux in the Ge substrate. As a result, less EHPs generation occurs. Simultaneously, the sub-bandgap absorbed radiative heat flux which does not contribute to the EHPs generation increases due to this spectral shift. Therefore, the system efficiency decreases. Conversely, when the temperature of the radiator increases, the spectral distribution shifts toward the higher frequency range. This spectral shift leads to the increase in system efficiency caused by the increase in the above-bandgap absorbed radiative heat flux and the decrease in the sub-bandgap heat losses. However, as the temperature continues to rise, the increase in system efficiency starts to slow down for the case of ABG+BSR since the sub-bandgap radiative heat flux is additionally decreased by the reflected photons. For the BSR configuration, the system efficiency continues to rise with the radiator temperature as the sub-bandgap absorbed radiative heat flux, or room for the sub-bandgap photon utilization, is higher compared to the ABG+BSR configuration. Overall, the enhanced above-bandgap and the suppressed sub-bandgap radiative heat fluxes lead to the continuously increasing system efficiency.

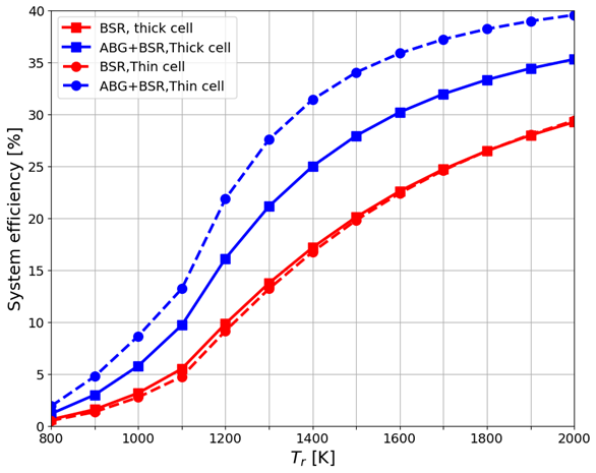

Fig. 8. System efficiencies of the NF-TPV converter for different radiator temperatures with 100% IQE.

As mentioned in section 2.2, the internal quantum efficiency of 100% is assumed. This assumption may overpredict the photogeneration rate at the higher radiator temperature where the spectral peak shifts further into the Ge bandgap. The far-field IQE of the Ge substrate [25] demonstrates near-ideal performance (i.e. close to 100%) across the frequency range from approximately the Ge bandgap frequency (~1.0042×10^{15} rad/s) to ~2.35×10^{15} rad/s. Beyond this range, the IQE drops significantly. However, for the radiator temperature of 1400 K, this drop in the IQE has negligible effect on the system efficiency. This is because the above-bandgap absorbed radiative heat flux in the Ge substrate diminishes to less than 10% of its peak that occurs near 1.2×10^{15} rad/s at the frequency around 2.0×10^{15} rad/s as shown in Fig. 2(b). However, for higher radiator temperatures, the consideration of the realistic IQE becomes crucial.

4. Concluding Remarks

The performance of the NF-TPV converter with the Tungsten radiator and the Germanium-based TPV cell are investigated in this study. An air-bridge gap is inserted between the Ge substrate and the back surface reflector to improve the performance of the converter by maximizing the sub-bandgap photon utilization, as it enhances the reflectivity in the sub-bandgap region. The effects of the air-bridge gap size on the radiative heat fluxes of the converter are investigated. The air-bridge gap is shown to improve the reflectivity at the interface between the Ge substrate and the air-bridge gap compared to the configuration with only the BSR leading to less amount of the sub-bandgap radiative heat flux reaching and being absorbed by the BSR. As a result, the converter's system efficiency is significantly improved. The optimum thickness of the air-bridge gap is determined to be 1300 nm, where the absorbed radiative heat flux in the BSR cannot be further minimized. The addition of the air-bridge gap increases the power output densities by 3.3% and 6.3% in the thick (i.e. t_{cell} = 175 μm cell) TPV cell and the thin (i.e. t_{cell} = 40 μm cell) TPV cell, respectively. The system efficiencies are significantly improved by 7.8% and 14.7% yielding efficiencies of 24.98% and 31.39% for the 175 μm cell and the 40 μm cell, respectively. The better performance is observed in the thin TPV cell due to the lower parasitic heat absorption. In addition, the analysis of the converter's performance under varying radiator temperature shows that the realistic IQE is important if the study is implemented at the higher radiator temperature. The findings in this study suggest that the air-bridge gap is the impactful strategy to enhance the system efficiency of the NF-TPV converter. Moreover, the approach is feasible for the Ge-based cells due to their relatively thicker substrate compared to thin-film cells providing strong structural support for the addition of the air-bridge gap. Lastly, the Ge substrate thickness significantly affects the converter's overall performance where the thinner substrate shows better system efficiency.

Acknowledgement

This work is supported by the Micro/Nano Electromechanical Integrated Device Research Unit, Faculty of Engineering, Chulalongkorn University, Thailand. In addition, computational resources for this work are provided by the NSTDA Supercomputer Center (ThaiSC) and the National e-Science Infrastructure Consortium.

References

[1] C. Amy, H. R. Seyf, M. A. Steiner, D. J. Friedman, and A. Henry, "Thermal energy grid storage using multi-junction photovoltaics," *Energy Environ. Sci.*, vol. 12, no. 1, pp. 334–343, Jan. 2019, doi: 10.1039/C8EE02341G

[2] L. M. Fraas, "Economic potential for thermophotovoltaic electric power generation in the steel industry," in *2014 IEEE 40th Photovoltaic Specialist Conference (PVSC)*, Denver, CO, USA, 2014, pp. 0766-0770, doi: 10.1109/PVSC.2014.6925031.

[3] Y. Wang, H. Liu, and J. Zhu, "Solar thermophotovoltaics: Progress, challenges, and opportunities," *APL Mater.*, vol. 7, no. 8, p. 080906, Aug. 2019, doi: 10.1063/1.5114829.

[4] K. Joulain, J.-P. Mulet, F. Marquier, R. Carminati, and J.-J. Greffet, "Surface electromagnetic waves thermally excited: Radiative heat transfer, coherence properties and Casimir forces revisited in the near field," *Surf. Sci. Rep.*, vol. 57, no. 3, pp. 59–112, May 2005, doi: 10.1016/j.surfrep.2004.12.002.

[5] M. Francoeur and M. Pinar Mengüç, "Role of fluctuational electrodynamics in near-field radiative heat transfer," *J. Quant. Spectrosc. Radiat. Transf.*, vol. 109, no. 2, pp. 280–293, Jan. 2008, doi: 10.1016/j.jqsrt.2007.08.017.

[6] S. Basu, Z. M. Zhang, and C. J. Fu, "Review of near-field thermal radiation and its application to energy conversion," *Int. J. Energy Res.*, vol. 33, no. 13, pp. 1203–1232, 2009, doi: 10.1002/er.1607.

[7] R. Mittapally et al., "Near-field thermophotovoltaics for efficient heat to electricity conversion at high power density," *Nat. Commun.*, vol. 12, no. 1, p. 4364, Jul. 2021, doi: 10.1038/s41467-021-24587-7.

[8] M. Gamel et al., "Highly reflective and passivated ohmic contacts in p-Ge by laser processing of aSiCx:H(i)/Al_2O_3/aSiC films for thermophotovoltaic applications," *Sol. Energy Mater. Sol. Cells*, vol. 265, p. 112622, Jan. 2024, doi: 10.1016/j.solmat.2023.112622.

[9] T. Nagashima, K. Okumura, and M. Yamaguchi, "A Germanium back contact type thermophotovoltaic cell," *AIP Conf. Proc.*, vol. 890, no. 1, pp. 174–181, Feb. 2007, doi: 10.1063/1.2711734.

[10] J. Fernández, F. Dimroth, E. Oliva, M. Hermle, and A. W. Bett, "Back surface optimization of Germanium TPV cells," *AIP Conf. Proc.*, vol. 890, no. 1, pp. 190–197, Feb. 2007, doi: 10.1063/1.2711736.

[11] P. Martín, V. Orejuela, A. Cano, I. García, A. Luque, and I. Rey-Stolle, "Cost-effective 23.2% efficient Germanium thermophotovoltaic converters for thermal batteries," *Cell Rep. Phys. Sci.*, vol. 5, no. 10, Oct. 2024, doi: 10.1016/j.xcrp.2024.102231.

[12] T. Inoue, K. Watanabe, T. Asano, and S. Noda, "Near-field thermophotovoltaic energy conversion using an intermediate transparent substrate," *Opt. Express*, vol. 26, no. 2, pp. A192–A208, Jan. 2018, doi: 10.1364/OE.26.00A192.

[13] D. Fan, T. Burger, S. McSherry, B. Lee, A. Lenert, and S. R. Forrest, "Near-perfect photon utilization in an air-bridge thermophotovoltaic cell," *Nature*, vol. 586, no. 7828, pp. 237–241, Oct. 2020, doi: 10.1038/s41586-020-2717-7.

[14] M. K. Arulanandam *et al.*, "GaAs thermophotovoltaic patterned dielectric back

contact devices with improved sub-bandgap reflectance," *Sol. Energy Mater. Sol. Cells*, vol. 238, p. 111545, May 2022, doi: 10.1016/j.solmat.2021.111545.
[15] S. M. Rytov, *Principles of Statistical Radiophysics 3*. Berlin, Heidelberg: Springer-Verlag Berlin Heidelberg, 2011.
[16] K. Chen, B. Zhao, and S. Fan, "MESH: A free electromagnetic solver for far-field and near-field radiative heat transfer for layered periodic structures," *Comput. Phys. Commun.*, vol. 231, pp. 163–172, Oct. 2018, doi: 10.1016/j.cpc.2018.04.032.
[17] J. Song, J. Han, M. Choi, and B. J. Lee, "Modeling and experiments of near-field thermophotovoltaic conversion: A review," *Sol. Energy Mater. Sol. Cells*, vol. 238, p. 111556, May 2022, doi: 10.1016/j.solmat.2021.111556.
[18] "NSM archive—Basic parameters of Germanium (Ge)." Ioffe Institute. Accessed: October 27, 2024. [Online]. Available: https://www.ioffe.ru/SVA/NSM/Semicond/Ge/
[19] P. Martín, V. Orejuela, C. Sanchez-Perez, I. García and I. Rey-Stolle, "Device architectures for Germanium TPV cells with efficiencies over 30%," in *2023 14th Spanish Conference on Electron Devices (CDE)*, Valencia, Spain, 2023, pp. 1-4, doi: 10.1109/CDE58627.2023.10339503.
[20] E. D. Palik, *Handbook of Optical Constants of Solids, Vol. 1*. San Diego, California: Academic Press, 1985.
[21] T. N. Nunley *et al.*, "Optical constants of Germanium and thermally grown Germanium dioxide from 0.5 to 6.6eV via a multisample ellipsometry investigation," *J. Vac. Sci. Technol. B*, vol. 34, no. 6, p. 061205, Sep. 2016, doi: 10.1116/1.4963075.
[22] M. Nedeljkovic, R. Soref, and G. Z. Mashanovich, "Predictions of free-carrier electroabsorption and electrorefraction in Germanium," *IEEE Photonics J.*, vol. 7, no. 3, pp. 1–14, Jun. 2015, doi: 10.1109/JPHOT.2015.2419217.
[23] A. D. Rakić, A. B. Djurišic, J. M. Elazar, and M. L. Majewski, "Optical properties of metallic films for vertical-cavity optoelectronic devices," *Appl. Opt.,* vol. 37, pp. 5271-5283, 1998.
[24] V. Liu and S. Fan, "S4: A free electromagnetic solver for layered periodic structures," *Comput. Phys. Commun.*, vol. 183, no. 10, pp. 2233–2244, Oct. 2012, doi: 10.1016/j.cpc.2012.04.026.
[25] E. Blanco et al., "Refractive indices and extinction coefficients of p-type doped Germanium wafers for photovoltaic and thermophotovoltaic devices," *Sol. Energy Mater. Sol. Cells*, vol. 264, p. 112612, Jan. 2024, doi: 10.1016/j.solmat.2023.112612.

Natkamon Pongtemsuk was born in Bangkok, Thailand. He received the B.Eng. in mechanical engineering from Chulalongkorn University, Thailand, in 2020. He is currently pursuing Master degree in mechanical engineering at Chulalongkorn University, Thailand.

Roytor Charoensin-O-Larn is a lecturer in the department of mechanical engineering, Chulalongkorn University, Bangkok, Thailand. He earned his Ph.D. in mechanical engineering from the University of Washington, USA in 2022.

Naphatsorn Vongsoasup is a lecturer in the department of mechanical engineering, Chulalongkorn University, Bangkok, Thailand. She received D.Eng. in mechanical engineering from the Institute of Science Tokyo, Japan in 2018. Since her graduate school, her research interest is energy conversion devices specifically thermophotovoltaic device. Her research focuses on improvement of TPV device performance through near-field effect and spectral control of radiative heat transfer.